Meteoritics & Planetary Science 41, Nr 11, 1705–1714 (2006)
Abstract available online at http://meteoritics.org

Titan's damp ground: Constraints on Titan surface thermal properties from the temperature evolution of the Huygens GCMS inlet

Ralph D. LORENZ[1, 3, 4*], Hasso B. NIEMANN[2], Dan N. HARPOLD[2], Stanley H. WAY[2], and John C. ZARNECKI[3]

[1]Lunar and Planetary Laboratory, The University of Arizona, 1629 East University Boulevard, Tucson, Arizona 85721, USA
[2]National Aeronautics and Space Administration, Goddard Space Flight Center, Greenbelt, Maryland 20771, USA
[3]Planetary and Space Science Research Institute, The Open University, Walton Hall, Milton Keynes, MK7 6AA, UK
[4]Present address: Space Department, Johns Hopkins University Applied Physics Laboratory, 11100 Johns Hopkins Road, Laurel, Maryland 20723, USA
*Corresponding author. E-mail: ralph.lorenz@jhuapl.edu

(Received 31 January 2006; revision accepted 09 June 2006)

Abstract–A simple thermal model is developed to determine the temperature history of the inlet tube of the Huygens probe gas chromatograph mass spectrometer (GCMS) after its fortuitous emplacement on the surface of Saturn's moon Titan. The model parameters are adjusted to match the recorded temperature history of a nearby heater, taking into account heat losses by conduction to the rest of the probe and to Titan's cold atmosphere. The model suggests that after impact when forced convective cooling ceased, the inlet temperature rose from ~110 K to an asymptotic value of only ~145 K. This requires that the inlet was embedded in a surface that acted as an effective heat sink, most plausibly interpreted as wet or damp with liquid methane. The data appear inconsistent with a tar or dry, fine-grained surface, and the inlet was not warm enough to devolatilize methane hydrate.

INTRODUCTION

The Huygens probe to Titan, part of the joint NASA/ESA Cassini mission, carried a gas chromatograph mass spectrometer (GCMS) that made composition measurements of the atmosphere during descent (Niemann et al. 2005). After surviving a relatively soft impact (Zarnecki et al. 2005) onto Titan's surface, the probe continued to operate and the GCMS continued to report mass spectra. The inlet of the instrument (Niemann et al. 2002) was heated to permit analysis of volatile surface materials, and indeed an increase in methane abundance relative to the atmosphere just above the surface was observed, suggesting that methane was released from the surface. Here we explore the thermal properties of the material from which the methane was released.

Onboard accelerometers suggest that the probe's descent speed of ~5 m/s was arrested over a vertical distance of ~15 cm with no major bounce, although some brief (~2 s) postimpact motion cannot be ruled out (Fulchignoni et al. 2005). On the other hand, study of the evolution of the Huygens postimpact radio signal strength (Perez-Ayucar et al. 2006) allows interferometric determination of the height of the probe antenna above the surface with a precision of better than ~10 cm, and this analysis appears to suggest that the base of the probe was lying on the surface (i.e., the eventual penetration depth was only 1–2 cm.) The impact dynamics may be reconciled with this postimpact position if impact began by contact with a number of the ~12 cm cobbles littering the landing site.

In any case, it seems most likely that the GCMS inlet (Fig. 1) was embedded in the surface substrate. This cannot be determined conclusively (one cannot rule out, for example, the pathological case of the inlet arriving above a hole or gully in the surface) but seems the most probable scenario, and we shall show that this appears to be supported by thermal analysis and by the detection of a novel assemblage of volatile materials after impact. The compounds detected included ethane (C_2H_6) and methane (CH_4), both liquids at Titan conditions (Niemann et al. 2005), as well as carbon dioxide (CO_2), cyanogen (C_2N_2), benzene (C_6H_6), and others.

To place the evolution of the volatiles into context (i.e., to understand the likely temperature history of the sample from which the volatiles were exsolved), we develop in this paper a thermal model of the inlet. In addition to documenting the thermal circumstances of volatile release, we show that the model itself constrains the thermal properties of the surface material and thereby its composition.

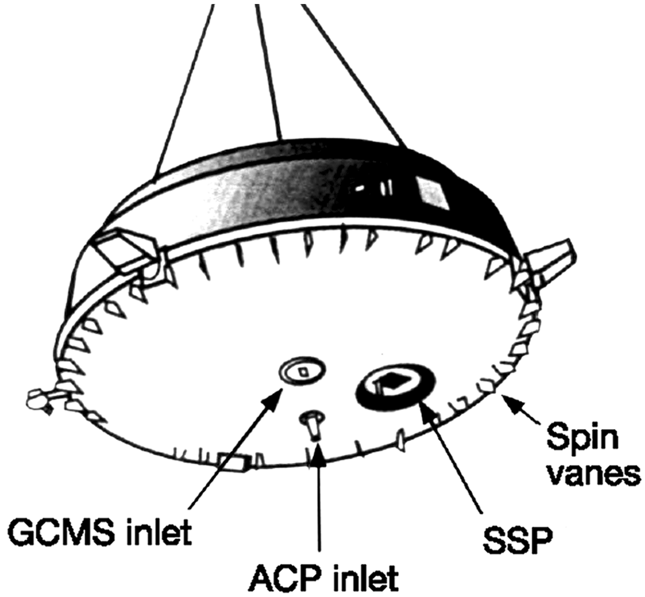

Fig. 1. A schematic view of the base of the Huygens probe showing the inlet location of the GCMS instrument.

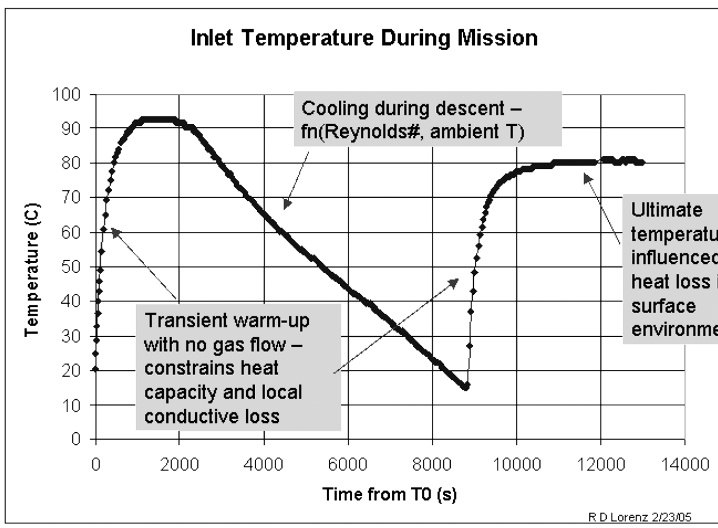

Fig. 2. The inlet heater temperature profile showing dramatic warming after impact at 8870 s.

FLIGHT DATA AND MODEL ARCHITECTURE

The Huygens GCMS inlet aperture was indirectly heated. Although its temperature was not measured directly, the heater to which the inlet was connected by some centimeters of pipework was monitored every few seconds by a thermistor and showed a dramatic warming after the probe landed on Titan's surface (Fig. 2).

There are several terms in the heat budget of the heater. First, there was a constant supplied power of 5 W. Some of this leaked conductively (heat flow *F1*, see later) to the rest of the GCMS instrument, which can be considered a large heat sink attached to the rest of the probe, and for which a thermal history can be assumed from housekeeping sensors. The remainder leaked to the environment through various direct and indirect paths. The changing conditions during descent are reflected in the changing heat loss terms and thus in the heater temperature profile.

The inlet heater's first recorded temperature about 9 s after *T0* is 20.4 °C. *T0* defines the start of the probe descent and corresponds to the fire command for the mortar for the pilot parachute. It occurred at 09:10:21 Universal Time on January 14, 2005. The temperature quickly rose to a flat-topped peak of ~92.8 °C between 1200 and 1900 s before declining steadily to 14.9 °C at impact (8870 s). At this point, the temperature rose sharply, reaching an asymptotic value of about 80 °C with a time constant of approximately one minute (Fig. 2).

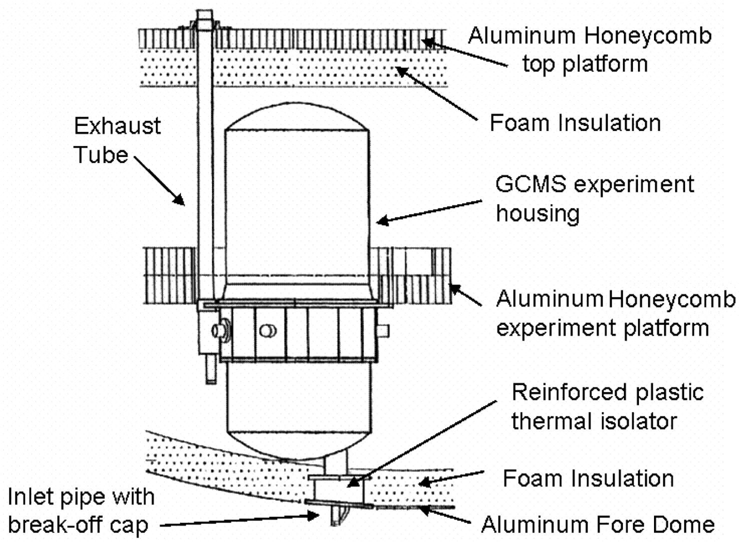

Fig. 3. A cross-sectional diagram of part of the Huygens probe showing the GCMS experiment and the structures to which it is attached. The GCMS experiment housing is 470 mm long. The inlet assembly is attached to the probe fore-dome by a largely hollow thermal isolator. The breakoff cap was removed at the beginning of descent.

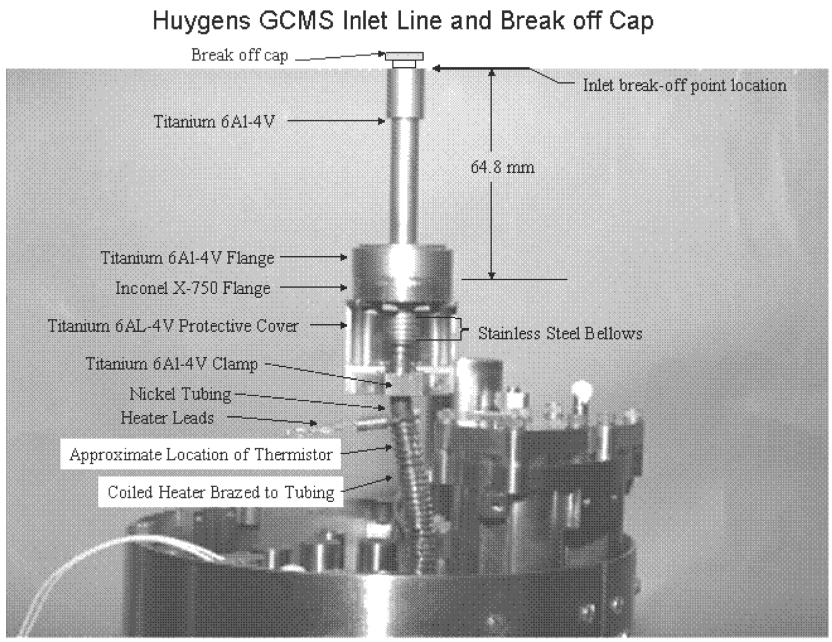

Fig. 4. The GCMS inlet assembly with the instrument casing and thermal isolator removed to show components between inlet pipe and thermistor location. The uppermost titanium inlet tube and flange sit inside the thermal isolator shown in Fig. 3. This view is inverted relative to Figs. 1 and 3; in flight, the inlet pipe points down into Titan.

In order to identify the temperature history of the inlet itself and its surrounds after impact, it is necessary to construct a model that captures the principal heat transfer processes and that can reproduce the descent temperature history of the heater. Inspection of the engineering drawings of the GCMS (Figs. 3 and 4) suggests that four nodes in the model are necessary. (Lower-order models were first attempted, but could not reproduce the flight data.) The four model nodes (Fig. 5) are:

1. The heater tube itself, which is of relatively low thermal mass, whose temperature history is known.
2. The probe "heat sink," which can be considered of infinite heat capacity and whose temperature is specified as a function of time from housekeeping sensors.
3. The inlet tube tip, which is exposed at the front of the probe. This inlet tube is of fairly robust construction, since it interfaced with a sealing mechanism with a ceramic breakoff cap.

Table 1. Model parameters.

Parameter	Symbol	Unit	Expected range	Tuned value	Comment
Heater power	*P*	W	5	5	Regulated heater current
Heat capacities					
Heater	*C1*	J/K	5–15	10	Nickel tube, plus heater Effective length between 2 and 7 cm
Flange	*C2*	J/K	20–50	25	Inconel flange plus titanium flange and surrounding parts
Inlet	*C3*	J/K	5–20	15	Titanium tube (effective length 2–5 cm)
Conductances					
Heater: probe	*R1*	W/K	0.02–0.1	0.045	Effective length of nickel tube plus heat leaks
Heater: flange	*R2*	W/K	0.02–0.1	0.02	Principally determined by bellows
Flange: inlet	*R3*	W/K	0.03–0.1	0.03	Titanium tube ~4 cm long
Heater temperature at *T0*		K	293	293	Fixed by first datapoint
Flange temperature at *T0*		K	220–300	250	Characteristic of other external probe elements
Inlet temperature at *T0*		K	220–300	250	Characteristic of other external probe elements
Heater pipe flow loss	*k1*	W/K	0.001–0.1	0.012	*Q1* = *k1**VFR*(*T_flange-T_heater*)
Flange pipe flow loss	*k2*	W/K	0.001–0.1	0.014	*Q2* = *k2**VFR*(*T_ambient-T_flange*)
Volume flow rate	*VFR*	m^3/s		0.0055ΔP	Poiseuille flow, assuming 1 cm diameter, 10 cm long pipe *P* is dynamic pressure; 6 Pa under main; 57 under stabilizer > 900 s
Inlet heat transfer to ambient atmosphere	*k3*	W/m^2K		0.37 $Re^{0.6}$	$Q3 = 4 \times 10^{-4}$*(*T_inlet-T_ambient*)**k3* Reynolds number defined for inlet diameter
Inlet peak temperature limit	*T_lim*	K	94–200	145	
Heat sink temperature	*T_probe*	K	250–300	290 + 10(*t/tf*)	Linear rise of 10 K over $0 < t < tf = 13000$ s
Atmospheric profile	Temperature, density versus altitude				Lellouch-Hunten profile (equivalent to Yelle nominal)
Descent profile	Altitude, velocity versus time				DTWG delivery 2

4. A flange between the heater and inlet. In an early version of the model, this flange was lumped together with the inlet tube; however, further consideration suggested that the thermal resistance of the inlet tube would be enough to somewhat decouple the flange and the inlet tip.

The heater assembly itself consists of a nickel tube about 7 cm long and 5 mm in diameter, with walls 0.5 mm thick. The upper end of this tube is connected to the instrument. The lower end is mated via a flexible stainless steel bellows (Miniflex SS-250-40-43) to a flange to which the inlet tube is fixed. The thermistor which records the temperature history is attached to the tube about 2 cm from the bellows.

The bellows mates to an Inconel flange, which is bolted to a titanium flange of the same diameter (30 mm). The titanium flange, inlet tube, and the inlet tip are all the same 50 g, 65 mm long metal part of Titanium 6Al-4V alloy, although they are considered separately in the model. In the model, we consider the inlet tube (which has thin walls) as a thermal resistance with negligible heat capacity, connecting two nodes, namely the inlet tip and the flange assembly. Since the inlet tube, heater pipe, and to a lesser extent the flange are continuous elements, the choice of element boundaries, conductivities, and heat capacities is somewhat arbitrary, although the construction details derived from engineering drawings (Dan Harpold, personal communication, 2005) place some basic constraints on their values. Table 1 summarizes the parameter ranges used.

In addition to the heat conduction paths between the nodes (*F1* heater to probe, *F2* heater to flange, and *F3* flange to inlet), heat is also lost to the environment. This is considered separately for each of the three main nodes *C1*–*C3*, and the corresponding heat transfers *Q1*–*Q3* are evaluated in the next section.

MODEL PARAMETERS

The baseline model parameters and values after tuning are summarized in Table 1. Although the model has several parameters that are known either poorly or not at all a priori, the descent has several different phases that permit the model to be tuned.

The initial inlet temperature is not known, but other sensors on or near the probe skin (e.g., Lorenz 2006) have initial temperatures of 250 K, so this seems a plausible starting value. The known initial value of the heater temperature, 293 K, is similar to many other internal items in the probe.

In a moving airstream, an object such as the exposed inlet is cooled with a heat transfer coefficient h that typically depends on the flow. Reynolds number Re mostly increases with time due to the increasing density of the air (the heat transfer coefficient varies as $Re^{0.6}$, where the Reynolds number is $DV\rho/\mu$, where D is the inlet diameter (~1 cm), V is the descent or windspeed, ρ is the atmospheric density (~5.4 kgm^{-3} near the surface), and μ is the atmospheric viscosity (8×10^{-6} Pa s). As the probe descends into denser air, the terminal velocity V decreases, but only as $\rho^{-0.5}$, and thus the Reynolds number and heat transfer coefficient both increase. Although the loss $Q3 = h \times \Delta T \times 1$ cm^2 is perhaps the dominant term affecting the inlet tip directly, it does not constitute the main heat loss mechanism from the system as a whole except for a brief period early during the descent.

The main loss is due to the gas flow through the instrument. In an arbitrarily long system of pipes acting as a heat exchanger, the gas flow will warm from the ambient temperature at which it is ingested into the system to the temperature of the pipes themselves. The heat loss rate is then $\rho c p \Delta T \times VFR$, where the volume flow rate VFR is given by viscous (Poisueille) pipe flow. The gas is assumed to warm to the pipe temperature in each section, thus for the first term $Q1$ (loss from the flange) $T = (T\_ambient\text{-}T\_flange)$ and for the second $Q2$ (loss from the heater) the gas has already been warmed to T_flange, and thus $T = (T\_flange\text{-}T\_heater)$.

The driving pressure ΔP is determined by the stagnation pressure on the base of the probe due to its descent. (In steady terminal descent, this pressure simply equals gravity multiplied by the ballistic coefficient β of the probe-parachute system $\beta = m/C_dA$ where m is the probe mass ~200 kg and A and C_d are the reference area and effective drag coefficient of the probe-parachute system). For the short descent under the main parachute, this pressure is ~6 Pa. Under the smaller stabilizer parachute, the dynamic pressure increases to 57 Pa. The labyrinth of pipes that controls the flow is not simple to describe: we therefore leave these terms as a lumped parameter $k3$ which we will set empirically.

Post impact, one might choose to manipulate the boundary condition $Q3$ by some model of heat transfer into the surface (e.g., conduction from a point source into a half space). However, for convenience, we simply allow the inlet to warm to some threshold temperature T_lim at which it is pinned, since this encapsulates the only reliable information from the model. Of course, in reality the temperature was not strictly pinned, but evolved depending on the balance of heat supply and loss. In practice this results in an evolution which has a transient whose character (undetectable in our data) depends on the details of the loss process, but which overall tends to yield an asymptotic temperature. Thus defining this asymptotic temperature, T_lim simplifies the modeling by decoupling the internal heat flows in the instrument model from the more complex but unconstrained environmental heat loss, which can then be studied separately.

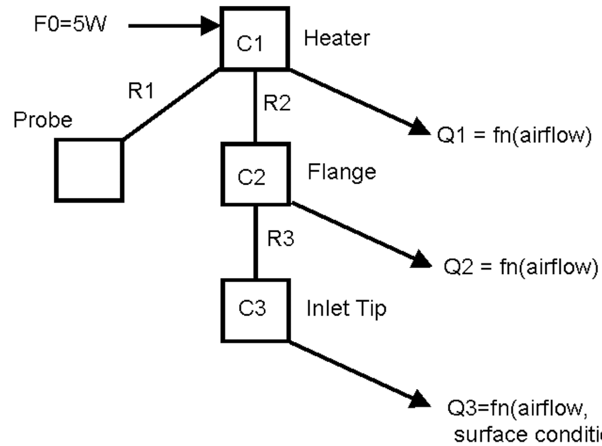

Fig. 5. A schematic of the model. Heat capacities *C1, C2,* and *C3* are connected via conduction paths *R2* and *R3*. *C1* also leaks via *R1* to the probe acting as an infinite heat sink. Internal flows *F1, F2,* and *F3* act along *R1, R2,* and *R3*. Heat is lost from each reservoir via gas flow losses *Q1, Q2*, and *Q3* which are a function of descent: these are set to zero in the first 50 s and after landing, except for *Q3* which has an imposed surface profile.

MODEL BEHAVIOR AND TUNING

Although it turns out that the transient heater temperature behavior, eye-catching though it may be (e.g., Fig. 2), is not diagnostic of external parameters, the various transients do constrain the model internal parameters, which in turn are required to interpret the steady-state conditions on the surface.

For example, the initial seconds of descent allow the isolation of the immediate paths around the heater. The breakoff caps which seal the inlet and exhaust pipes were only removed by pyrotechnic firing at 50 s. Up to that time, there was no gas flowing into the instrument, and thus the only heat transfers were the heater power and conductive leaks, plus the convective cooling ($Q3$) of the inlet tube exposed to the airflow.

This period therefore constrains the conductive paths from and the heat capacity of the heater. The temperature increases linearly at about 0.28 K/s. Given the 5 W heater power, this implies an effective heat capacity $C1$ of no more than 5/0.28

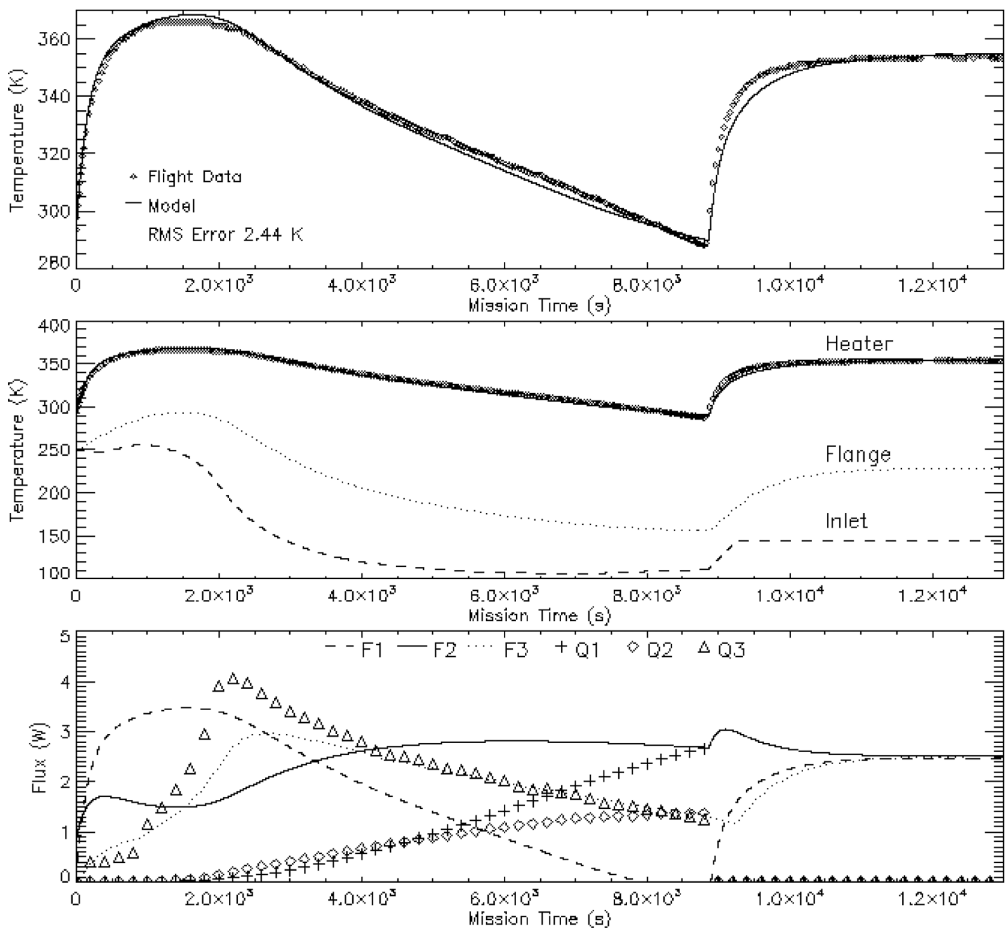

Fig. 6. Tuned model performance: heater model temperature matches flight data fairly well. Model flange and inlet temperatures are shown, together with model conductive heat paths *F1–F3* and external flows *Q1–Q3*.

= 16 J/K. This may be compared with the heat capacity estimated by construction of ~10 J/K. The difference is accounted from additional thermal masses in contact with the heater (e.g., the heater cable, mounting hardware not shown in construction drawings, etc.) and by heat losses.

After 100 s, the temperature increase becomes 0.13 K/s. This implies that the gas flow is responsible for a heat loss of up to (0.28–0.13) × *C1* ~ 0.15*16 = 2.4 W. Another diagnostic point is that immediately after impact. The last record prior to impact (8869 s) is 27.1 °C at 8878 s. The following datapoint, 36.8 °C at 8921 s, implies that the heater temperature—again without advective heat losses—is rising at 0.22 K/s. The fact that this rise is lower than during the flow-free initial phase implies that the conductive heat loss either to the probe or flange must be higher than during that phase. A lower flange temperature seems most likely. From 500–1300 s, the temperature progressively and smoothly flattens out to just above 365 K. There is not a profound discontinuity at the parachute changeover at 900 s; if one fits the profile at that time by two line segments, the rate drops from about 0.014 K/s to zero.

During the main part of descent (phase 2; 2000–8800 s; e.g., Fig. 6), the steady drop in temperature is due to the progressive increase in atmospheric density—a slight inflection may be indicative of the tropopause temperature minimum. The slope requires that the dominant heat transfer be proportional to Reynolds number (i.e., density) as when the ambient air warms completely to the pipe temperature on flowing through—if it is alternatively assumed that the heat is only lost by forced convective cooling of the exposed inlet itself (i.e., ~density^0.6), the shape of the curve cannot be reproduced well. Since this period is so strongly leveraged by the somewhat arbitrary choice of cooling, this period cannot usefully constrain any of the other parameters such as the internal conduction paths.

MODEL RESULTS

After tuning, the model indeed reproduces the flight data quite well (Fig. 6), capturing all the qualitative behaviors and yielding an RMS error of only ~2.5 K. Although it is possible that other combinations of parameters may yield comparably

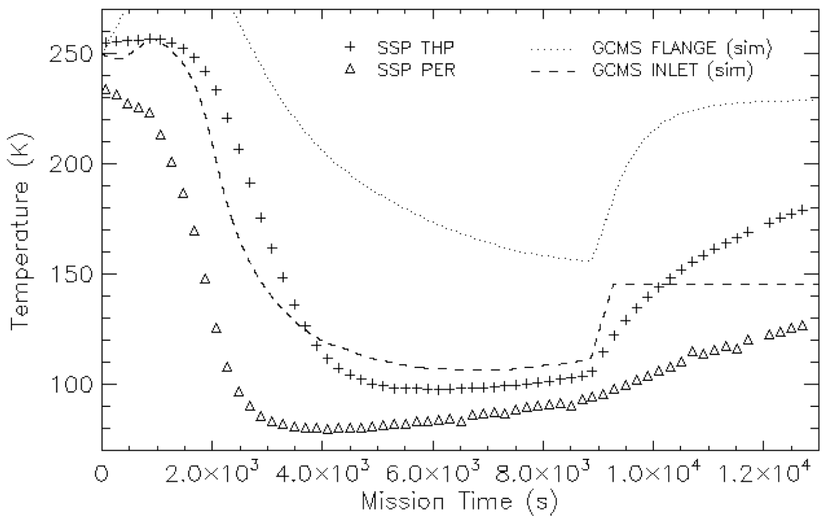

Fig. 7. The temperature evolution of the GCMS inlet model (dashed line) compared with measurements from two nearby SSP sensors exposed to the Titan environment. PER was fairly well coupled to the environment and stayed rather cold, while THP was warmed by a larger heat leak through the SSP top hat foam after impact. The generally similar behavior of the inlet model and THP suggests the model is plausible.

good fits, extensive experimentation has failed to indicate plausible parameter sets. It seems likely that further refinement of the model might only be worthwhile if additional data became available, from laboratory tests on the engineering model instrument, for example.

The rapid rise of the heater temperature is not matched by the flange and inlet, which start at much lower temperatures and are slowed primarily by the flange heat capacity. The inlet, flange, and heater temperatures would continue to rise after impact unless heat was removed (*Q3*) from the inlet somehow. In the model result above, this is simply achieved by setting *Q3* = *F3* once a threshold temperature is reached. The threshold *T_lim* is adjusted to make the asymptotic heater temperature agree with data.

This approach may be justified as follows. At the end of the mission, as during the descent around 1500 s, the heater temperature profile is flat, over a period comparable with the flange time constant (*C2/R2* ~1000 s). The system as a whole is therefore in balance. To a first approximation, then, on the surface heat is being lost from the inlet at a rate (~2.5 W) comparable to the loss to gas flow at 1500 s. A possible small change in probe heat sink temperature may influence the required inlet loss, such that *T_lim* may not be constrained to better than 10 K or so. But otherwise, unless the model configuration is modified by some ad hoc modification to a parameter at impact (e.g., if the bellows tore open—however, there is no indication that any change of any sort occurred at mpact), this result (*T_lim* ~145 ± 10 K) is robust. Put another way, with other parameters held fixed, changes in *T_lim* of >10 K lead to errors in the asymptotic temperature of the order of 3 K, and a degradation of the overall RMS error from ~2.4 to ~2.9 K. One may attempt to correct the asymptotic behavior by adjusting other parameters, but these alter the goodness of fit elsewhere and the overall RMS error does not decrease. Thus, temperatures outside the range 130–160 K are difficult to reconcile with the model.

A "sanity check" on the model result may be obtained by comparison with other flight temperatures (Fig. 7). A couple of sensors in the Surface Science Package (SSP) "top hat" structure, open to the bottom of the probe (Fig. 1) but not exposed to as vigorous a freestream airflow during descent, are shown below. These show very similar gross behavior, although both get cooled more than the GCMS inlet during the deep, cold part of descent since they lack direct heating. After impact, their temperatures rise due to the modest heat leak, but more slowly than the inlet, since their heating is less. The similarity of these observed temperature histories gives some confidence that the inlet model predictions are reasonable.

SURFACE ENVIRONMENTAL RESULTS AND INTERPRETATION

The detailed history of the surface material temperature cannot be directly recovered due to the low-pass-filtering imposed by the resistances between the heater and inlet and the thermal inertia of the flange. However, the asymptotic behavior can be constrained—the inlet temperature rises to *T_lim* ~145 K, while losing around 2.5 W to the environment.

This appears to be incompatible with the inlet being simply exposed to the air. Free-convection cooling would not remove the heat fast enough—a heat transfer coefficient of some (2.5/[50 K*1 cm^2]) = 500 Wm^{-2}K^{-1} would be needed, yet well-known engineering correlations (e.g., Holman 2002) suggest the conditions would support only ~10 Wm^{-2}K^{-1}.

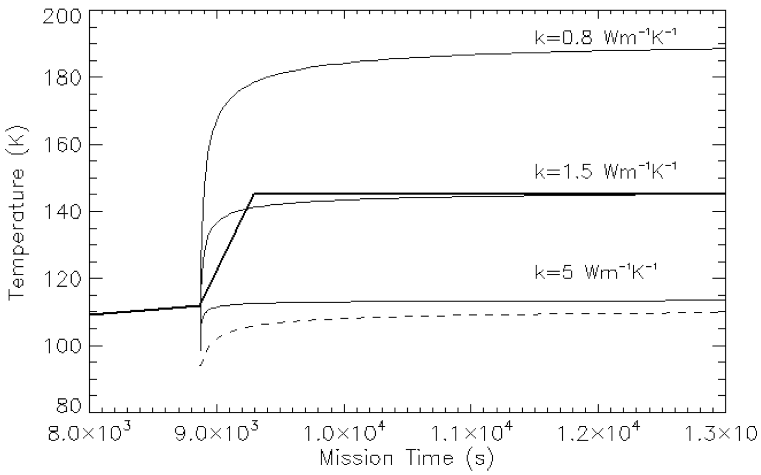

Fig. 8. The temperature at the inlet surface for constant 2.5 W heating and various assumed thermal conductivities (solid lines). The thick line shows the temperature profile expected from the model of the inlet heater system discussed in the previous sections. A thermal conductivity of the surface material of ~1.5 $Wm^{-1}K^{-1}$ agrees quite well. The corresponding temperature history 1 cm from the inlet is shown in the dashed line; the heating is evidently quite localized. Note that since this is the material in contact with the inlet, not the inlet itself, the histories start at the surface temperature of 94 K.

Forced convection by wind does not appear viable as a heat loss mechanism, since this would lead to more rapid cooling of the probe as a whole: ndeed, the slow cooling post-impact has been used to derive a constraint on near-surface winds (Lorenz 2006). Thus, a surface heat sink appears to be required. Either heat is drawn away from the inlet by conduction into a cold surface material, or evaporation of volatile surface material, or both.

Considering evaporation first, it might be expected that dipping into liquid hydrocarbons might pin the temperature at 94 K (lower than permitted by the model results above). However, boiling heat transfer is complicated—the heat transfer may in fact be retarded by the self-shielding due to bubble formation such as the Leidenfrost effect (e.g., Holman 2002). Heat transfer rates from water (at ~273 K) into liquid ethane, methane, and nitrogen have been measured (in the context of determining evaporation rates in the event of spillage of liquefied natural gas tankers, Drake et al. 1975) at around 20 kW/m^2, or 2 W/cm^2. Given the ~1 cm^2 area of the inlet, it would appear quite possible to support boiling on immersion in surface liquids with the observed heat loss.

A pure liquid surface is of course incompatible with the impact dynamics and other data from the probe: the surface was mechanically solid, even if the heat transfer may have been dominated by evaporation of liquid. Since the liquid composition (ethane/methane/nitrogen mix) and thus its vapor pressure curve is unknown, and its contact may be influenced by solid materials around the inlet, more sophisticated quantitative analysis of evaporation is probably futile.

Alternatively, we may consider a purely solid surface with heat loss only by conduction. There are well-known analytic solutions for many such heat transfer problems. The most appropriate here is a continuously heated spherical heat source in an infinite space with given thermal properties. By symmetry this is equivalent to the problem at hand, a half-space with an approximately hemispherical source, with a factor of 2 applied in the source term. Note that the boundary condition at the surface is not pinned at the atmospheric temperature of 94 K, but is allowed to increase since the probe's thick insulation isolates the subsurface material from above. The resultant solution (Carslaw and Jaeger 1959), with nomenclature modified for the present problem, is

$$\Delta T = \left(\frac{Q}{8\pi\kappa r a}\right)\left\{2(\kappa t/\pi)^{0.5}\left[e^{-(r-a)^2/4\kappa t} - e^{-(r+a)^2/4\kappa t}\right] - |r-a|\,erfc\frac{|r-a|}{2(\kappa t)^{0.5}} + |r+a|\,erfc\frac{|r+a|}{2(\kappa t)^{0.5}}\right\} \quad (1)$$

where $Q = 2*Q3/(\rho*Cp)$ with ρ is the material density and Cp its specific heat capacity, r is the radial distance of the point under consideration, a is the radius of the heat source (here the inlet outer radius ~ 0.005 m), t is time since impact, and κ is the thermal diffusivity of the material. The thermal diffusivity relates to the conductivity k as $\kappa = k/\rho Cp$. *Erfc* is the complementary error function.

Although the three material properties cannot be independently constrained, some useful conclusions can be drawn. First, most nonmetals have a ρCp product of 1–2 × 10^6 $Jm^{-3}K^{-1}$. The lower end of this range seems more likely, given the mechanical properties inferred from the impact dynamics (Zarnecki et al. 2005) suggesting a tarry sludge or sand-sized ice. We thus adopt 1–2 × 10^6 $Jm^{-3}K^{-1}$. With ρCp chosen, we are left with k as the free parameter.

As noted previously, the transient behavior immediately after the impact cannot be captured in the model so no effort is made to tune this (if a small, directly heated element were emplaced into the surface, its heating characteristics could permit, independently, the thermal conductivity and thermal diffusivity). The asymptotic temperature behavior depends only on the conductivity (Fig. 8) and to match the flight data requires k ~1.5 $Wm^{-1}K^{-1}$, or given the uncertainty in the overall model, $1 < k < 2$ $Wm^{-1}K^{-1}$. To a first order, the asymptotic temperature increase is ~$80/k$. There is a direct correspondence between the asymptotic model inlet temperature and the model heater temperature—i.e., an increase of 5 K in the inlet requires and increase of 5 K in the heater, which is constrained by observations.

Solid and liquid organic materials tend to have $0.2 < k < 0.3$ $Wm^{-1}K^{-1}$, thus a tar (the "crème brulee hypothesis") seems incompatible with the observed temperature history. Solid ice at 94 K has a conductivity of ~5 $Wm^{-1}K^{-1}$, while solid ammonia-rich ice has a conductivity of ~2 $Wm^{-1}K^{-1}$(Lorenz and Shandera 2001). Clathrate hydrates or ices like CO_2 tend to have $k < 1$ $Wm^{-1}K^{-1}$, e.g., Ross and Kargel (1998). A solid surface (of any kind of ice) appears to be excluded by the relatively soft impact forces, so we must consider the lower conductivity of granular ices.

Dry sand (made predominantly of quartz, with bulk k ~3–5 $Wm^{-1}K^{-1}$) has a typical conductivity of 0.3 $Wm^{-1}K^{-1}$. If we consider a "sand" made of water ice, and assume the same particle size and contact physics, the conductivity of the sand is proportional to that of the bulk material and thus a dry water-ice sand at 94 K on Titan would also have k ~0.4 $Wm^{-1}K^{-1}$ (heat transfer is dominated by the solid component—although because Titan's atmosphere is somewhat thicker it adds only ~0.1 $Wm^{-1}K^{-1}$). Measurements of pure granular methane clathrate (Waite et al. 2002) and its temperature dependence suggest a conductivity at 94 K of ~0.5 $Wm^{-1}K^{-1}$, although this is with a confining pressure of some 24.8 MPa—loose, unconfined clathrate sand would have somewhat lower conductivity. A dry powder of organic material would similarly be insulating. Thus all "dry" sands appear to have conductivities too low to be compatible with the inlet temperature history.

However, moist or wet terrestrial sand can have effective conductivities of 0.25–2 $Wm^{-1}K^{-1}$ and 2–4 $Wm^{-1}K^{-1}$, respectively (some convection doubtless also plays a role in increasing the effective conductivity). By analogy, on Titan water-ice sand (or indeed solid organic granules, CO_2 ice, clathrates, etc.) saturated with hydrocarbon liquids could have the desired thermal properties. The relative amounts and composition cannot be meaningfully constrained since evaporation (already shown to be not incompatible with the heat flux needed) will play a role in the heat transfer from the inlet.

It is worth pointing out also that a dry deposit of sand made from methane clathrate could not provide the methane vapor detected postimpact: the dissociation pressure of clathrate (Sloan 1998) is given by $P(\text{kPa}) = \exp[38.98–8533.8/T(\text{K})]$, or 10^{-10} bar at 150 K. Thus methane in a liquid form appears to be required both to provide the observed vapor release, and the required heat transfer. The release of methane does not require that the liquid making the surface damp be pure or even predominantly methane. If the atmosphere (with a methane mixing ratio of about 5%, equivalent to a relative humidity of ~50–60%) were in thermodynamic equilibrium with a surface liquid, this would imply that the proportions of methane and involatile constituents such as ethane be roughly equal.

Hydrocarbons like liquid methane have a latent heat of 4×10^5 Jkg^{-1}, and thus a deposition of 2.5 W over an hour or so yields 10^4 J, or enough heat to evaporate about 25 g of material. In reality, the amount evolved was probably much less, perhaps limited by how well liquid was wicked or flowed through granular material to the inlet. One might infer that since the evolved methane did not increase continuously post impact, but rather leveled off, that the material in immediate contact with the inlet may have "dried out" of methane. The history of a point 1 cm from the inlet (Fig. 7) shows that only a small volume of material was substantially heated, so such an apparent dessication is reasonable.

The nondetection of water vapor does not argue for the presence or absence of water ice at the landing site, since the inlet was never warm enough to give water a significant vapor pressure. CO_2 has a vapor pressure of about 5 mbar at 145 K, and thus the CO_2 detection is compatible with the inlet temperature history. Phase changes of other materials (e.g., melting of hydrocarbons and nitriles) may also have occurred, but since latent heats of melting are modest compared with those of evaporation and melting would tend to reduce the degree of contact with the inlet, it seems most plausible that evaporation of liquid methane was the dominant heat transfer process.

A separate study (Lorenz 2006) demonstrates that the heat leaking from the probe interior through its foam insulation and aluminum fore-dome was minimal and thus did not contribute to the production of vapors sensed by GCMS. An analysis of vapor-liquid equilibrium for various surface liquid compositions and thermal properties, together with vapor transport by diffusion, may allow the interpretation of the postimpact abundance histories of the various components. However, such an analysis is beyond the scope of the work here.

CONCLUSIONS

Although some modest model uncertainties remain, it seems clear that the inlet was considerably lower in temperature than the heater, both at impact and as the inet and heater warmed up afterward. Model results appear reasonable when compared with other data. The transient heater behavior cannot be directly interpreted, but allows model constraints to be derived which in turn allow the interpretation of the asymptotic behavior on the surface.

The postimpact temperature evolution requires an effective heat sink on the ground. Neither free convection (were the inlet exposed to free air) nor thermal conduction by organic material such as tar on the surface can remove heat quickly enough. A dry “sand” made of ice, methane clathrate or other materials is similarly inadequately conductive. A sand or clay (i.e., sand-, silt-, or clay-sized particles made of water ice, clathrate, or organics) made moist or wet with hydrocarbon liquid appears the most prominent candidate to explain the postimpact thermal behavior. The inlet did not get warm enough to liberate the observed methane by clathrate decomposition—some liquid methane had to be in contact with the inlet. Experimental simulation of the various scenarios may be instructive.

This study demonstrates the potential scientific utility of even simple housekeeping sensors. Evidently, data from such sensors and documentation to facilitate their interpretation should form part of the scientific archive. A sensor directly on the inlet would of course have made this modeling exercise unnecessary, but the heater temperatures provide an adequate constraint when supported by construction information and nearby temperatures.

Acknowledgments–This work was supported by NASA via the Cassini project. We acknowledge the many workers in the Huygens team in ESA, NASA, industry, and academia who both made these measurements possible and helped in understanding the resting state of the probe.

Editorial Handling—Dr. A. J. Timothy Jull

REFERENCES

Carslaw H. S. and Jaeger J. C. 1959. *Conduction of heat in solids.* Oxford: Oxford University Press. 510 p.

Drake E. M., Jeje A. A., and Reid R. C. 1975. Transient boiling of liquefied cryogens on a water surface. I. Nitrogen, methane, and ethane. *International Journal of Heat and Mass Transfer* 18: 1361–1368.

Fulchignoni M., Ferri F., Angrilli F., Ball A. J., Bar-Nun A., Barucci M. A., Bianchini G., Bettanini C., Borucki W., Colombatti G., Coradini W., Coustenis A., Debei S., Falkner P., Fanti G., Flamini E., Gaborit V., Hamelin M., Grard R., Harri A. M., Hathi B., Jernej I., Leese M. R., Lehto A., López-Moreno J. J., Mäkinen T., McDonnell J. A. M., McKay C. P., Molina-Cuberos G., Neubauer F. M., Pirronello V., Rodrigo R., Saggin B., Schwingenschuh K., Seiff A., Simões F., Svedhem H., Tokano T., Towner M. C., Trautner R., Withers P., and Zarnecki J. C. 2005. In situ measurements of the physical characteristics of Titan’s environment. *Nature* 438:785–791.

Holman J. P. 2002. *Heat transfer,* 9th ed. New York: McGraw-Hill. 688 p.

Ross R. G. and J. S. Kargel. 1998. Thermal conductivity of solar system ices, with special reference to Martian polar caps. In *Solar system ices,* edited by Schmitt B., de Bergh C., and Festou M. Dordrecht, The Netherlands: Kluwer Academic Publishers. pp. 33–62.

Lorenz R. D. 2006. Thermal interaction of the Huygens probe with the Titan environment: Surface windspeed constraint. *Icarus* 182:559–566.

Lorenz R. D. and Shandera S. E. 2001. Physical properties of ammonia-rich ice application to Titan. *Geophysical Research Letters* 28:215–218.

Niemann H. B., Atreya S. K., Bauer S. J., Biemann K., Block B., Carignan G. R., Donahue T. M., Frost, R. L., Gautier D., Haberman J. A., Harpold D. N., Hunten D. M., Israel G., Lunine J. I., Mauersperger K., Owen T. C., Raulin F., Richards J. E., and Way S. H. 2002. The gas chromatograph mass spectrometer for the Huygens probe. *Space Science Reviews* 104:553–591.

Niemann H. B., Atreya S. K., Bauer S. J., Carignan G. R., Demick J. E., Frost R. L., Gautier D., Haberman J. A., Harpold D. N., Hunten D. M., Israel G., Lunine J. I., Kasprzak W. T., Owen T. C., Paulkovich M., Raulin F., Raaen E., and Way S. H. 2005. Huygens probe gas chromatograph mass spectrometer: The atmosphere and surface of Titan. *Nature* 438:779–784.

Pérez-Ayúcar M., Lorenz R. D., Floury N., Prieto R., and Lebreton J-.P. Forthcoming. Surface properties of Titan from post-landing reflections of the Huygens radio signal. *Journal of Geophysical Research.*

Sloan E. D., Jr. 1998. Physical/chemical properties of gas hydrates and application to world margin stability and climatic change. In *Gas hydrates: Relevance to world margin stability and climate change*, edited by Henriet J.-P. and Mienert J. London: Geological Society. pp. 31–50.

Waite W. F., deMartin B. J., Kirby S. H., Pinkston J., and Ruppel C. D. 2002. Thermal conductivity measurements in porous mixtures of methane hydrate and quartz sand. *Geophysical Research Letters* 29, doi:10.1029/2002GL015988.

Zarnecki J C., Leese M. R., Hathi B., Ball A. J., Hagermann A., Towner M. C., Lorenz R. D., McDonnell T., Green S. F., Patel M. R., Ringrose T. J., Rosenberg P. D., Atkinson K. R., Paton M., Banaskiewicz M., Clark B. C., Ferri F., Fulchignoni M., Ghafoor N A. L., Kargl G., Svedhem H., Delderfield J., Grande M., Parker D. J., and Challenor P. 2005. A soft solid surface on Titan at the Huygens landing site as measured by the Surface Science Package (SSP). *Nature* 438:792–795.